Supplemental Information

Ultrasmall episymbiotic Saccharibacteria suppresses gingival inflammation and bone loss through host bacterial modulation

Otari Chipashvili, Daniel R. Utter, Joseph K. Bedree, Yansong Ma, Fabian Schulte, Gabrielle Mascarin, Yasmin Alayyoubi, Deepak Chouhan, Markus Hardt, Felicitas Bidlack, Hatice Hasturk, Xuesong He, Jeffrey S. McLean, Batbileg Bor

Figure S1. Related to Figure 1.

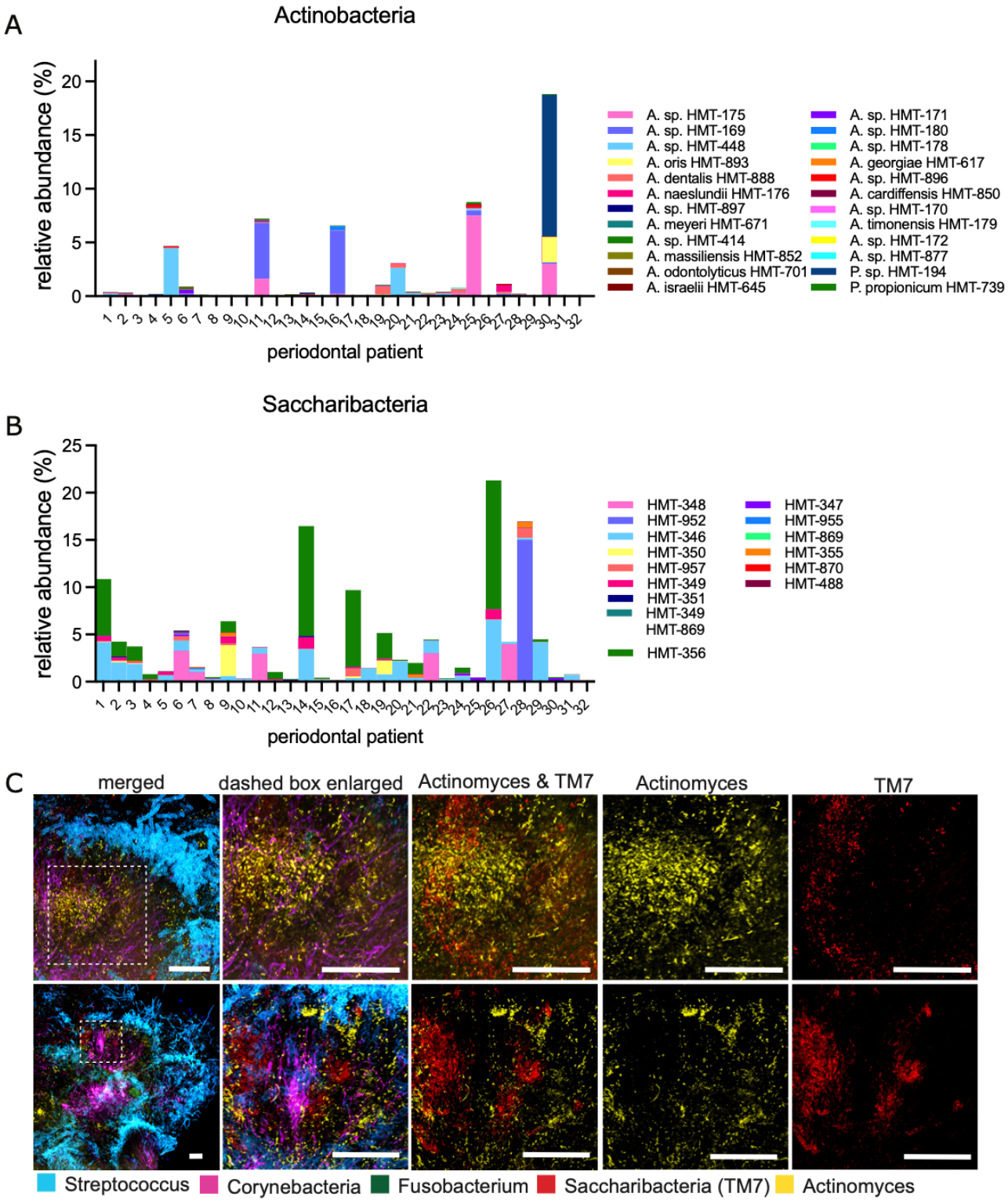

Figure S1. TM7 bacteria in periodontal plaque. Related to Figure 1. (A) Actinobacteria and (B) TM7 bacteria 16S rRNA profiling for individual samples for 32 patient cohort. Some samples contained TM7 bacteria up to 60% of the total relative abundance. (C) Additional FISH-Spectral imaging sample images of periodontal plaque from separate patients. Six bacteria were stained with genus-specific probes. All scale bars are 30 μm.

Figure S2. Related to Figure 2.

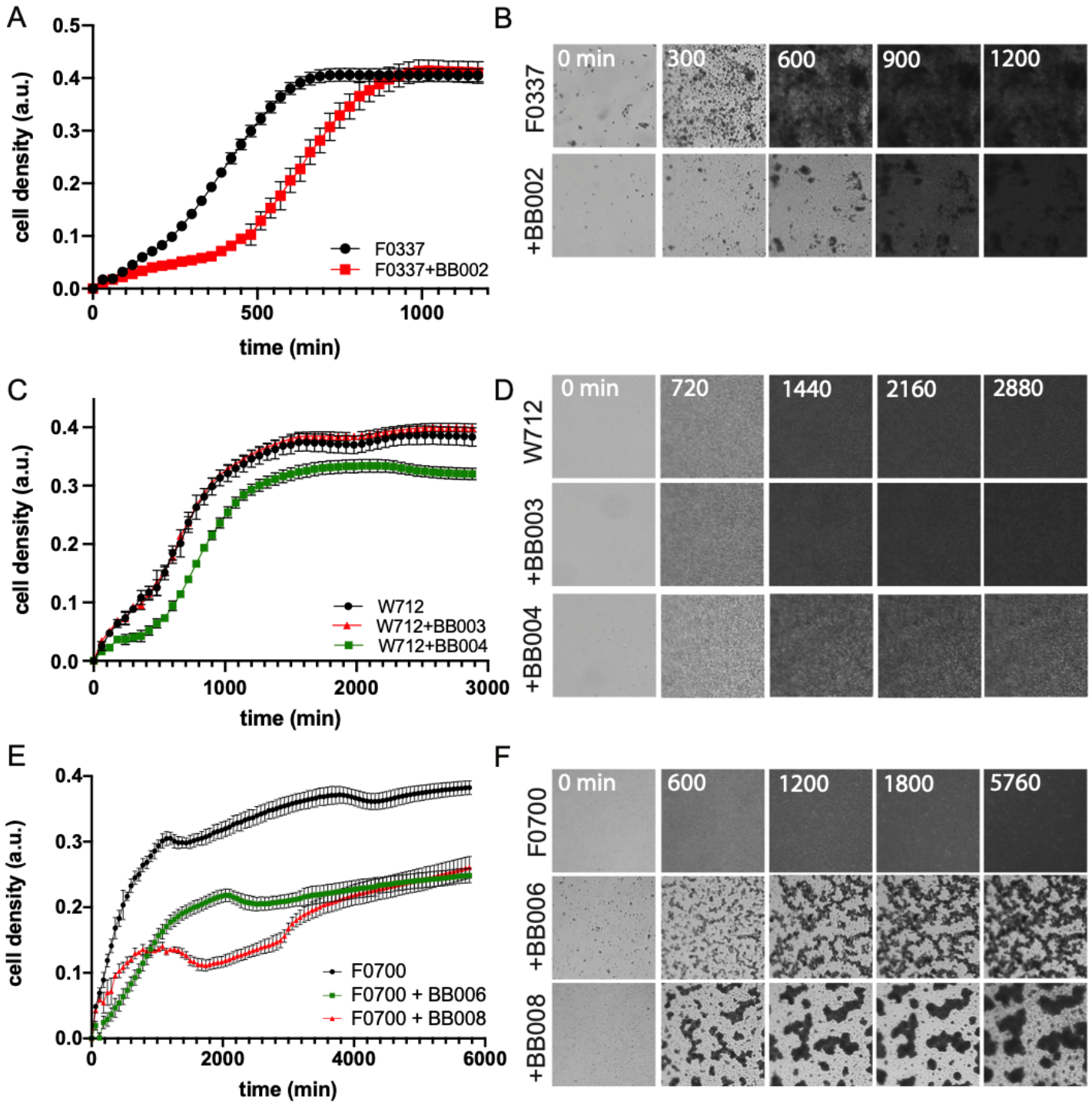

Figure S2. Growth curve of TM7 and their host bacteria. Related to Figure 2. (A, C, E) Cell density measurement (arbitrary unit, a.u.) was graphed across time (minutes) in each mono (black) or cocultures (green or red) using OcelloScope (see STAR methods). (B, D, F) Individual representative images of a particular culture at indicated times are shown, which correlates with the graphs in A, C, and E.

Figure S3. Related to Figure 3.

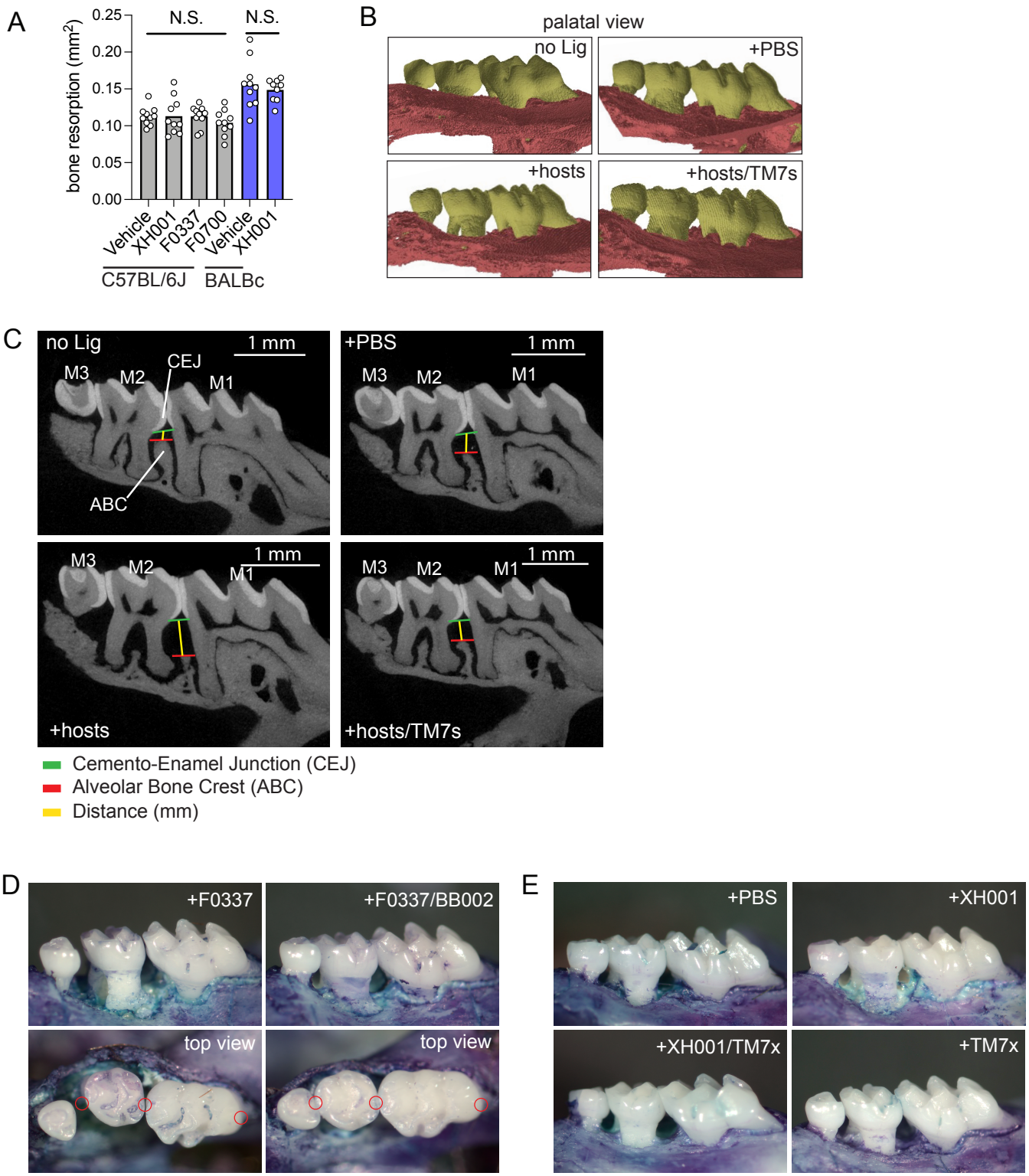

Figure S3. Ligature-induced periodontitis model. Related to Figure 3. (A) Quantification of bone resorption in the oral infection model after antibiotic treatment and repeated inoculation by indicated bacteria. Results are shown as mean (bar) ± SD. Each dot indicates an individual ligature (n = 6-10). N.S., not significant by Mann-Whitney U test. (B) 3D images of maxillae taken with a microCT scanner to show the differences in bone resorption in the periodontitis ligature model from the palatal view. The buccal view is shown in Figure 3A. (C)

The distance between the cemento-enamel junction (CEJ) and the alveolar bone crest (ABC) was measured between groups using microCT image section. Molars 1-3 are shown as M1-M3. (D) Representative images of the bone loss observed in F0337 host alone and F0337 with BB002 from Figure 3E. Top row is plane of view from the buccal side while bottom row is view from top of the molars. Red circles indicate disruption of teeth alignment. (E) Representative buccal view of maxillary molars of PBS, XH001, TM7x/XH001 and TM7x groups that is quantified in Figure 3E.

Figure S4. Related to Figure 3.

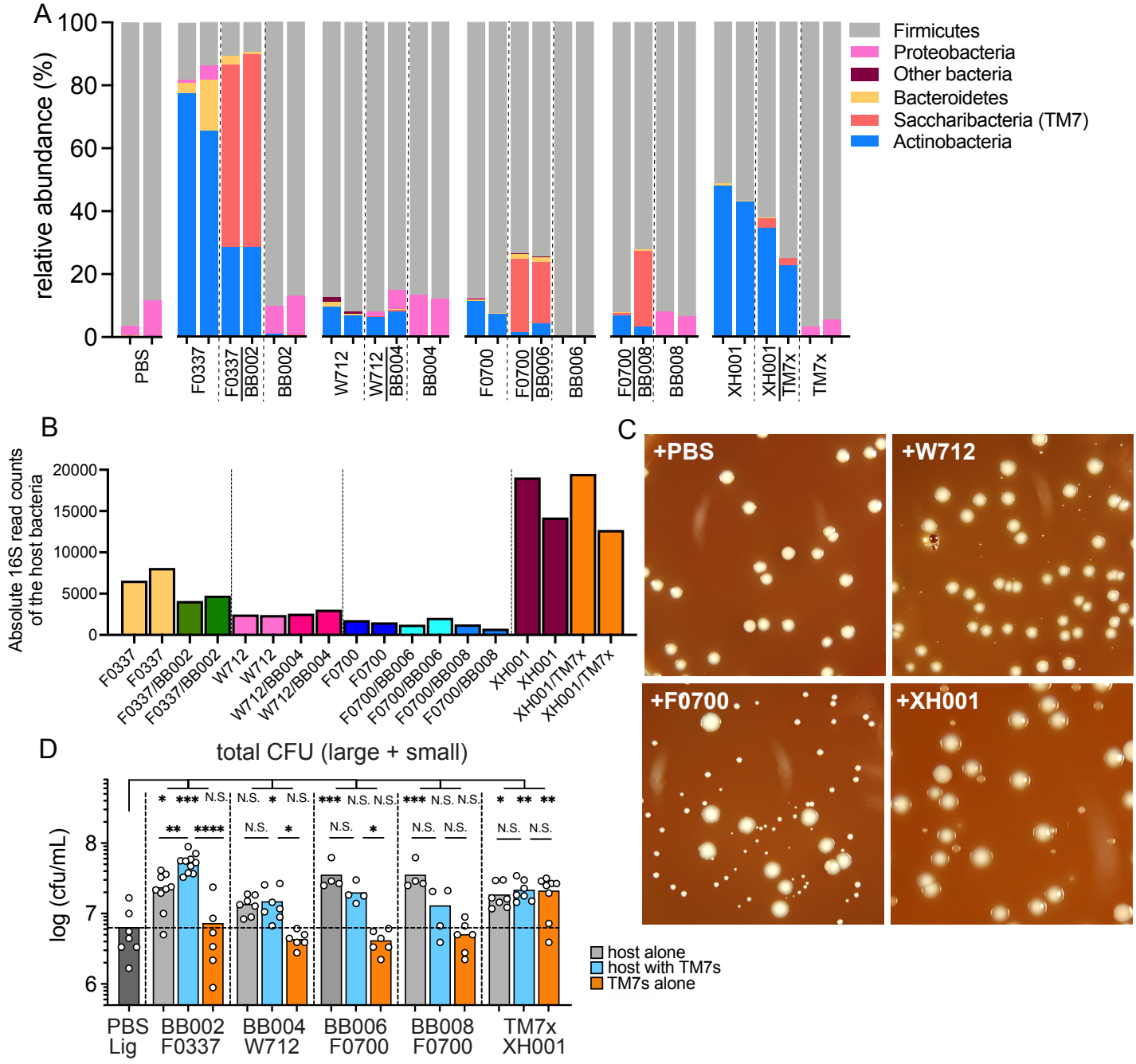

Figure S4. Ligature microbiome and their analysis. Related to Figure 3. (A) 16S rRNA relative abundance of ligature microbiome across different culture infections were analyzed. For each ligature microbiome group, two independent experiments were conducted and shown in the bar graph. (B) Absolute read counts of the 16S rRNA specific to TM7 or host bacteria were plotted from the sequencing study in panel A. Each matching color represent duplicate experiments from the same group. When analyzing this data, we compared only within groups and not between groups due to technical reasons (see methods). Further supporting information for this graph can be found in Table S6. (C) Representative images of the colonies that result from plating the bacteria that were obtained from the ligatures after extraction from the mouse oral cavity. In groups where host bacteria were added to the ligature, we observe slow growing “small” colonies. By PCR, small colony forming units (CFUs)

were confirmed to be host bacteria and the large CFUs were mostly native oral bacteria that dominated by *Firmicutes.* (D) Quantification of total CFUs, including small and large, that were recovered from each ligature after the experiment in Figure 3E. Results are shown as mean (bar) ± SD. Each dot indicates an individual ligature (n = 4-10). N.S., not significant; *p < 0.05, **p < 0.01, ***p < 0.001, ****p < 0.0001 by one-way ANOVA followed by Bonferroni post hoc test.

Figure S5. Related to Figure 4.

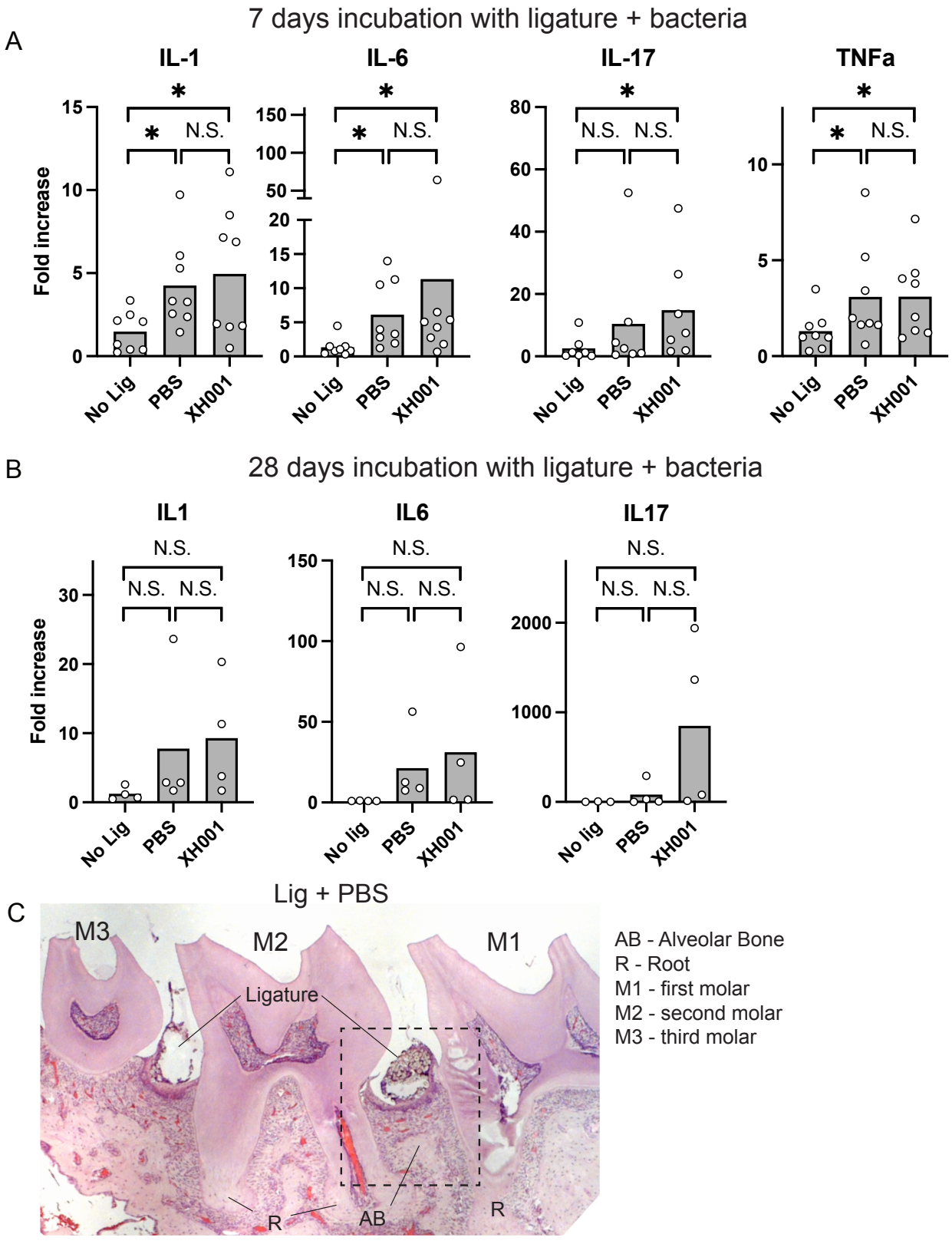

Figure S5. Tissue cytokine and histology analysis. Related to Figure 4. (A-B) Periodontitis was induced in C57BL6 mice by using the ligature model with indicated different groups. Ligatures were kept in the mice for 7 or 28 days and the mRNA expression of IL-1, IL-6, IL-17 and TNFα from the gingiva was extracted and quantified

by qPCR. Results are shown as mean (bar) ± SD. Each dot indicates an adjacent tissue from individual ligature (n = 4-10). N.S., not significant; *p < 0.05, **p < 0.01, ***p < 0.001, ****p < 0.0001 by one-way ANOVA followed by Bonferroni post hoc test. (C) Histology tissue section that is stained with H&E showing area of analysis in Figure 4. Three molars (M1-M3) are clearly visible, and we targeted the area between M1 and M2 (dashed black box). Ligatures were kept in place during the histology section to show their location.

Figure S6. Related to Figure 6.

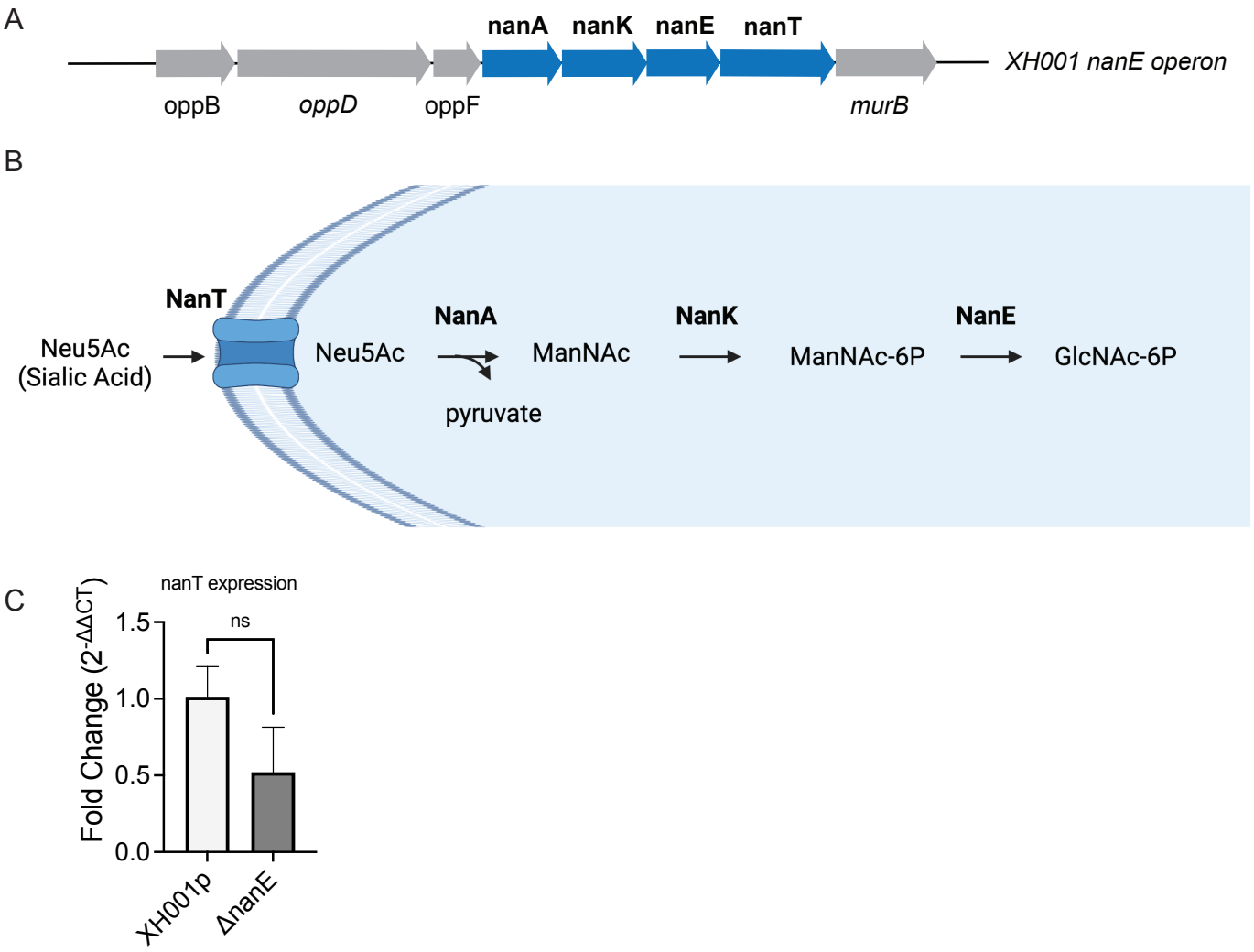

Figure S6. ***NanE* gene operon characterization. Related to Figure 6.** (A) Gene analysis of the XH001 genome revealed full set of *NanE* gene operon (*nanA, nanK, nanT*). (B) *NanE* operon is crucial for transportation and metabolisms of mammalian sialic acid, which is shown by cartoon model. (C) Quantification of nanT expression level in XH001p and *nanE* mutant using RT-qPCR with 16S rRNA gene as a baseline. The experiment was done with three biological replicates with standard deviation (error bar) depicting the variation. N.S., not significant with student t-test.

Table S1. TM7 is associated with numerous inflammatory diseases. Related to Introduction.

Body site	Disease type	References
Human Oral Cavity	gingivitis	Al-Kamel et al., 2019, J Oral Micro. 1:1608141 Huang et al., 2011, BMC Oral Heath. 11:33
	smoking	Duan et al., 2017, J Periodontol. 12:1297-1308 Ganesan et al., 2017, ISME J. 9:2075-2089
	halitosis	Kazor et al., 2003, J Clin Microbol. 2:558-663 Seerangaiyan et al., 2017, J Breath Res. 3:036010
	leukocyte adhesion deficiency I	Moutsopoulos et al., 2015, Plos Path. 3:e1004698
	peri-implantitis	Yu et al., 2019, Clin Oral Implant Res. 8:760-776
	invisalign/fixed-appliace induced alterations	Wang et al., 2019, Am J Orthod Den Orthop. 5:633-640
	periodontitis	Griffen et al., 2012, ISME J. 6:1176-1185 Abusleme et al., 2013, ISME J. 5:1016-1025 Galimanas et al., 2014, Microbiome. 2:32 Papapanou et al., 2020, J Periodontol. 1:S56-S67 Wei et al., 2019, Front Cell Infect Micro. 9:53
Other Human body sites	vaginosis	Fredricks et al., 2005, N Engl J Med, 18:1899-1911
	preterm birth	Fettweis et al., 2019, Nat Med, 6:1012-1021
	pelvic inflammatory disease	Haggerty et al., 2020, Sex Transm Dis.
	cervical cancer	Tango et al., 2020, Sci Rep. 16:10(1):9720
	inflammatory bowel disease	Kuehbacher et al., 2008, J Med Microbiol. 57:1569-1576 Qi et al., 2020, Genomics.
	ulcerative colitis	Zakerska-Banaszak et al., Sci Rep. 11:2166
	various lung diseases	Cheng et al., 2020, Transl Lung cancer Res. 3:693-704 Lee et al., 2016, Lung Cancer Amst Neth. 102:89-95
	neutrophilic asthma	Yang et al., 2018, BioMed Res Int. 9230234
	traveler's diarrhea	Zhu et al., 2018, Microbiome. 08:6(1):201
	Sjogren's syndrome	Wu et al., 2019, Chin J Integr Med. 9:654-662
	gastric carcinogenesis	Wang et al., 2020, Front Microbiol. 11:997
Rodent model	Colitis	Elinav et al., 2011, Cell. 5:745-757 Kang et al., 2013, Plos One. 8(10):e76520
	irritable bowel syndrome	Wang et al., 2018, Chin Med. 13:63
	colon cancer	Sivaprakasam et al., 2020, Biochem J. 19:3867-3883

Table S2. Host bacteria and their growth conditions for Saccharibacteria isolation. Related to Figure 2.

Strain name	Species	eHOMD HMT #	Media	Gas Temperature conditions used	Strain source
XH001	Actinomyces odontolyticus	701	BHI*	microaerophilic^, 37°C	He et al. 2015
W712	Actinomyces meyeri	671	BHI	microaerophilic^, 37°C	Forsyth Institute Strain Collection
F0337	Actinomyces species	171	BHI	microaerophilic^, 37°C	Forsyth Institute Strain Collection
F0386	Actinomyces species	170	BHI	microaerophilic^, 37°C	Forsyth Institute Strain Collection
F0700	Pseudopropionibacterium propionicum	739	TSBY**:RPMI***:FBS****	microaerophilic^, 37°C	Forsyth Institute Strain Collection
F0333	Actinomyces species	850	BHI	microaerophilic^, 37°C	Forsyth Institute Strain Collection
ORNL-0100	Cellulosimicrobium cellulins		TSBY:RPMI:FBS	microaerophilic^, 37°C	Mircea Podar strain
ORNL-0104	Actinomyces species	897	TSBY:RPMI:FBS	microaerophilic^, 37°C	Mircea Podar strain
ATCC35568	Actinomyces meyeri	671	BHI	microaerophilic^, 37°C	ATCC Global Bioresource Center

*BHI: Brain Heart Infusion
**TSBY:Trypticase Soy Broth, Yeast Extract (ATCC-1823)
***RPMI: Gibco RPMI 1640 media
****FBS: Fetal Bovine Serum
^microaerophilic condition corresponds to 2% oxygen, 5% CO2 balanced with nitrogen
HMT: Human Microbiome Taxon (part of eHOMD)

Table S3. Cultivated Saccharibacteria strains. Related to Figure 2.

Strain name	HMT#	% identity	Host Bacterial strains	Patient #	Isolation location	Conducted mouse experiment	Growth conditions^
BB002	957	99.7	*Actinomyces* sp. strain F0337 (HMT-171)	1	subgingival	yes	BHI*, micro
BB003	352	99.9	*Actinomyces* sp. strain W712 (HMT-671)	2	subgingival	no	BHI, micro
BB004	488	97.8	*Actinomyces* sp. strain W712 (HMT-671)	3	subgingival	yes	BHI, micro
BB006	955	99.8	*Pseudopropionibacterium propionicum* strain F0700 (HMT-739)	2	subgingival	yes	TSBY, micro
BB008	488	98	*Pseudopropionibacterium propionicum* strain F0700 (HMT-739)	3	subgingival	yes	TSBY**, micro
TM7x	952	100%	Actinomyces odontolyticus (HMT-701)	healthy	saliva	yes	BHI, micro

*BHI: Brain Heart Infusion medium
**TSBY:Trypticase Soy Broth, Yeast Extract (ATCC-1823)
^microaerophilic condition correspond to 2% oxygen, 5% CO2 balanced with nitrogen
Human Microbiome Taxon (part of HOMD)

Table S5. Primers used to create genetic deletion of cbp2 and nanE gene. Related to Figure 6.

Primer Name	Primer Sequence	Primer #
XH001Δcbp2 Up fragment F1	5'-AACGTCCAGCCCGCCAAGTCG-3'	1
XH001Δcbp2 Up fragment R1	5'-CTGAGCGGGACTCTGGGGTTCGCCGACTTCTCCTTCTATCGTCA-3'	2
XH001Δcbp2 Kan fragment F1	5'-TGACGATAGAAGGAGAAGTCGGCGAACCCCAGAGTCCCGCTCAG-3'	3
XH001Δcbp2 Kan fragment R1	5'-GGTGTGGGCCTCGCCTACGGGCCTGCAGCCAAGCTAGCTTCAC-3'	4
XH001Δcbp2 Dn fragment F1	5'-GTGAAGCTAGCTTGGCTGCAGGCCCGTAGGCGAGGCCCACACC-3'	5
XH001Δcbp2 Dn fragment R1	5'-GGGCAGCGGATCCTTGAGCGTG-3'	6
XH001ΔnanE Up fragment F1	5'GCCTCGTCGATTTTCTTATACCCC-3'	7
XH001ΔnanE Up fragment R1	5'-CTGAGCGGGACTCTGGGGTTCGCGGTGAACTCCTATGCGTGCA-3'	8
XH001ΔnanE Kan fragment F1	5'-TGCACGCATAGGAGTTCACCGCGAACCCCAGAGTCCCGCTCAG-3'	9
XH001ΔnanE Kan fragment R1	5'-CACTGTCCCAACAGCGACAGGACCTGCAGCCAAGCTAGCTTCAC-3'	10
XH001ΔnanE Dn fragment F1	5'-GTGAAGCTAGCTTGGCTGCAGGTCCTGTCGCTGTTGGGACAGTG-3'	11
XH001ΔnanE Dn fragment R1	5'-ACGACCGCACCGGTGAAGG-3'	12
XH001Δcbp2 5' Junction F1	5'-GCGAAAATGCCCTAAAGTAGTC-3'	13
XH001Δcbp2 5' Junction R1	5'-CGTGATATTGCTGAAGAGCTTG-3'	14
XH001ΔnanE 5' Junction F1	5'-GTATCACGGCCTGGTACGAC-3'	15
XH001ΔnanE 5' Junction R1	5'-ATCAGGATGATCTGGACGAAGA-3'	16
XH001Δcbp2 mRNA Primer 1	5'-GCCTCGTCCAACTCTGAGAC-3'	17
XH001Δcbp2 mRNA Primer 2	5'-GGATCGACGACCTTGATGTT-3'	18
XH001Δcbp2 mRNA Primer 3	5'-AAGGTCGGCATTAACGTGTC-3'	19
XH001Δcbp2 mRNA Primer 4	5'-ATACGCGAAGGTCTGCTTGT-3'	20
XH001Δcbp2 mRNA Primer 5	5'-CGTGGATGTCAACCAGAATG-3'	21
XH001Δcbp2 mRNA Primer 6	5'-GCTCGGAATCACTCTTGGAG-3'	22
XH001ΔnanE mRNA Primer 1	5'-AACCTGAAGGGCAAGCTCAT-3'	23
XH001ΔnanE mRNA Primer 2	5'-TTCCACAGCAGCCTTAAACC-3'	24
XH001 16s mRNA Primer 1	5'-GCGGAGCATGCGGATTA-3'	25
XH001 16s mRNA Primer 2	5'-AACGTGCTGGCAACATAGGG-3'	26
XH001 nanT gene primer 1 (RT-qPCR)	5'-GTGGATGGCTACGGCTACTC-3' (primer efficiency 103.3%)	27
XH001 nanT gene primer 2 (RT-qPCR)	5'GTGAAGGTGATGCGCAGCAGC-3' (primer efficiency 103.3%)	28